Science Advances
AAAS

advances.sciencemag.org/cgi/content/full/6/10/eaaz0525/DC1

Supplementary Materials for

Computational and experimental performance of CRISPR homing gene drive strategies with multiplexed gRNAs

Samuel E. Champer, Suh Yeon Oh, Chen Liu, Zhaoxin Wen, Andrew G. Clark, Philipp W. Messer, Jackson Champer*

*Corresponding author. Email: jc3248@cornell.edu

Published 4 March 2020, *Sci. Adv.* **6**, eaaz0525 (2020)
DOI: 10.1126/sciadv.aaz0525

The PDF file includes:

Other Supplementary Material for this manuscript includes the following:

(available at advances.sciencemag.org/cgi/content/full/6/10/eaaz0525/DC1)

Data S6 (Microsoft Excel format). Fly phenotype counts and analysis for the two-gRNA drive with close target sites.
Data S7 (Microsoft Excel format). Fly phenotype counts and analysis for the two-gRNA drive.
Data S8 (Microsoft Excel format). Fly phenotype counts and analysis for the three-gRNA drive.
Data S9 (Microsoft Excel format). Fly phenotype counts and analysis for the four-gRNA drive.

SUPPLEMENTAL INFORMATION

Supplementary Methods

Plasmid construction. The starting plasmids pCFD3 (*33*) (Addgene plasmid #49410) and pCFD5 (*31*) (Addgene plasmid #73914) were kindly supplied by Simon Bullock, and starting plasmids IHDyi2 (*12*), and BHDgN1a (*15*), and p3xP3-dsRedv2 (*15*) were constructed in our previous studies. Plasmid digests were conducted with restriction enzymes from New England Biolabs (HF versions, when possible). PCR was performed with Q5 Hot Start DNA Polymerase (New England Biolabs), and DNA oligos and gBlocks were obtained from Integrated DNA Technologies. Gibson assembly of plasmids utilized Assembly Master Mix (New England Biolabs), and plasmids were transformed into JM109 competent cells (Zymo Research). Plasmids used for injections were purified using the ZymoPure Midiprep kit (Zymo Research). Cas9 gRNA target sequences were found with CRISPR Optimal Target Finder (*34*). The following tables show the DNA fragments used for Gibson Assembly of each plasmid.

pgRNAtRNA	*Template*	*Oligo/Enzyme 1*	*Oligo/Enzyme 2*
PCR Product	pCFD5	CFDg_1_F	CFD_1_R
PCR Product	pCFD5	CFD_2_F	CFDg_2_R

AHDgg1t	*Template*	*Oligo/Enzyme 1*	*Oligo/Enzyme 2*
PCR Product	pgRNAtRNA	CFD_1_F	CFD_1_R
PCR Product	pgRNAtRNA	CFD_2_F	CFD5_2_R
PCR Product	none	EGFP1tt_gRNA_F	EGFP1t_gRNA_R

TTTgRNA	*Template*	*Oligo/Enzyme 1*	*Oligo/Enzyme 2*
PCR Product	p3xP3-EGFP	pBBtRNA_1_F	pBB_1_R
PCR Product	p3xP3-EGFP	pBB_2_F	pBBtRNA_2_R
PCR Product	pCFD3	gRNAtRNA_F	gRNAtRNA_R

TTTgRNAt	*Template*	*Oligo/Enzyme 1*	*Oligo/Enzyme 2*
PCR Product	p3xP3-EGFP	pBBtRNA_1_F	pBB_1_R
PCR Product	p3xP3-EGFP	pBB_2_F	pBBtRNA_2_R
PCR Product	AHDgg1t	gRNAtRNA_F	gRNAtRNA_R

TTTgRNAtRNAi	*Template*	*Oligo/Enzyme 1*	*Oligo/Enzyme 2*
PCR Product	p3xP3-EGFP	pBBtRNA_1_F	pBBtRNA_2_R
PCR Product	AHDgg1t	gRNAtRNA_F	EGFP1t_gRNA_R
PCR Product	pCFD3	CFD_1_F	gRNAtRNA_R

BHDgg1c	*Template*	*Oligo/Enzyme 1*	*Oligo/Enzyme 2*
PCR Product	pCFD3	CFD_1_F	CFD_1_R
PCR Product	pCFD3	CFD_2_F	CFD35_2_R
PCR Product	none	EGFP2_gRNA_F	EGFP2_gRNA_R

TTTgU1	*Template*	*Oligo/Enzyme 1*	*Oligo/Enzyme 2*
PCR Product	TTTgRNA	CFD_1_F	CFD35_2_R
PCR Product	none	EGFP1_gRNA_F	EGFP1_gRNA_R

TTTgU1t	*Template*	*Oligo/Enzyme 1*	*Oligo/Enzyme 2*
PCR Product	TTTgRNAtRNAi	CFD_1_F	CFD5_2_R
PCR Product	none	EGFP1t_gRNA_F	EGFP1_gRNA_R

TTTgU2	*Template*	*Oligo/Enzyme 1*	*Oligo/Enzyme 2*
PCR Product	TTTgRNAtRNAi	EGFP4_23_F	EGFP4_41_R
PCR Product	TTTgRNAt	EGFP4_12_F	EGFP4_12_R

TTTgU2s	*Template*	*Oligo/Enzyme 1*	*Oligo/Enzyme 2*
PCR Product	TTTgRNAtRNAi	EGFP4_41_F	EGFP4_41_R
PCR Product	TTTgRNAt	EGFP4_12_F	EGFP4_34_R

TTTgU3	*Template*	*Oligo/Enzyme 1*	*Oligo/Enzyme 2*
PCR Product	TTTgRNAtRNAi	EGFP4_34_F	EGFP4_41_R
PCR Product	TTTgRNAt	EGFP4_12_F	EGFP4_12_R
PCR Product	TTTgRNAt	EGFP4_23_F	EGFP4_23_R

TTTgU4	*Template*	*Oligo/Enzyme 1*	*Oligo/Enzyme 2*
PCR Product	TTTgRNAtRNAi	EGFP4_41_F	EGFP4_41_R
PCR Product	TTTgRNAt	EGFP4_12_F	EGFP4_12_R
PCR Product	TTTgRNAt	EGFP4_23_F	EGFP4_23_R
PCR Product	TTTgRNAt	EGFP4_34_F	EGFP4_34_R

TTTacU1	*Template*	*Oligo/Enzyme 1*	*Oligo/Enzyme 2*
PCR Product	TTTgRNA	acgRNA_1_F	pBB_1_R
PCR Product	TTTgRNA	pBB_2_F	acgRNA_2_R

TTTacU4	*Template*	*Oligo/Enzyme 1*	*Oligo/Enzyme 2*
PCR Product	TTTgRNAtRNAi	ACG4_41_F	ACG4_41_R
PCR Product	TTTgRNAt	ACG4_12_F	ACG4_12_R
PCR Product	TTTgRNAt	ACG4_23_F	ACG4_23_R
PCR Product	TTTgRNAt	ACG4_34_F	ACG4_34_R

ATSacG	*Template*	*Oligo/Enzyme 1*	*Oligo/Enzyme 2*
PCR Product	p3xP3-EGFP	pBB2_c_F	pBB2_c_R
PCR Product	Genomic DNA	AutoC_Left_F	AutoC_Left_R
PCR Product	p3xP3-EGFP	EGFP_c_F	EGFP_c_R
PCR Product	Genomic DNA	AutoC_Right_F	AutoC_Right_R

BHDgN1ci1	*Template*	*Oligo/Enzyme 1*	*Oligo/Enzyme 2*
Plasmid Digest	BHDgN1a	KpnI	AscI
PCR Product	ATSacG	EGFPacLeft_F	EGFPacLeft_R
PCR Product	BHDgN1a	Cas9Nos3c_F	Cas9Nos3_R

BHDgN1c	*Template*	*Oligo/Enzyme 1*	*Oligo/Enzyme 2*
Plasmid Digest	BHDgN1ci1	AgeI	DraIII
PCR Product	BHDgg1c	U6_3_gRNA1_v4_F	EGFPc_U6_3_gRNA1_R
PCR Product	ATSacG	EGFPacRight_F	EGFPacRight_R

BHDgN1cv2	*Template*	*Oligo/Enzyme 1*	*Oligo/Enzyme 2*
Plasmid Digest	BHDgN1c	NotI	StuI
PCR Product	ATSacG	b1v2_F	b1v2_R

AHDgN1i1	*Template*	*Oligo/Enzyme 1*	*Oligo/Enzyme 2*
Plasmid Digest	BHDgN1cv2	KpnI	NheI
PCR Product	p3xP3-dsRedv2	EGFPacLeft_F	G1Left_R

AHDgN1	*Template*	*Oligo/Enzyme 1*	*Oligo/Enzyme 2*
Plasmid Digest	AHDgN1i1	MluI	DraIII
PCR Product	TTTgU1t	gRNA_P10_F	gRNA_EGFP1_R
PCR Product	ATSacG	EGFP1Right_F	EGFPacRight_R

BHDgN1cv3	*Template*	*Oligo/Enzyme 1*	*Oligo/Enzyme 2*
Plasmid Digest	AHDgN1	MluI	XbaI
PCR Product	TTTgU1	gRNA_P10_F	gRNA_EGFP1v2_R

THDgN1	*Template*	*Oligo/Enzyme 1*	*Oligo/Enzyme 2*
Plasmid Digest	AHDgN1i1	MluI	DraIII
PCR Product	TTTgU1t	gRNA_P10_F	gRNA_EGFP4_R
PCR Product	ATSacG	EGFP4Right_F	EGFPacRight_R

AHDgN2	*Template*	*Oligo/Enzyme 1*	*Oligo/Enzyme 2*
Plasmid Digest	AHDgN1i1	MluI	DraIII
PCR Product	TTTgU1t	gRNA_P10_F	gRNA_EGFP4_R
PCR Product	ATSacG	EGFP4Right_F	EGFPacRight_R

AHDgN2s	*Template*	*Oligo/Enzyme 1*	*Oligo/Enzyme 2*
Plasmid Digest	AHDgN2	MluI	AgeI
PCR Product	TTTgU2s	gRNA_P10_F	gRNA_EGFP2_R
PCR Product	AHDgN1	EGFP2Right_F	EGFPacRg2_R

AHDgN3	*Template*	*Oligo/Enzyme 1*	*Oligo/Enzyme 2*
Plasmid Digest	AHDgN1i1	MluI	DraIII
PCR Product	TTTgU3	gRNA_P10_F	gRNA_EGFP4_R
PCR Product	ATSacG	EGFP4Right_F	EGFPacRight_R

AHDgN4	*Template*	*Oligo/Enzyme 1*	*Oligo/Enzyme 2*
Plasmid Digest	AHDgN1i1	MluI	DraIII
PCR Product	TTTgU4	gRNA_P10_F	gRNA_EGFP4_R
PCR Product	ATSacG	EGFP4Right_F	EGFPacRight_R

FACacN	*Template*	*Oligo/Enzyme 1*	*Oligo/Enzyme 2*
Plasmid Digest	BHDgN1c	StuI	XbaI
PCR Product	none	acN_F	acN_R

FACacN1	*Template*	*Oligo/Enzyme 1*	*Oligo/Enzyme 2*
Plasmid Digest	BHDgN1c	StuI	XbaI
PCR Product	TTTacU1	U6_3_gRNA1_v4_F	gRNA_f_R

FACacN1	*Template*	*Oligo/Enzyme 1*	*Oligo/Enzyme 2*
Plasmid Digest	BHDgN1c	StuI	XbaI
PCR Product	TTTacU4	U6_3_gRNA1_v4_F	gRNA_f_R

Construction primers

Acg4_12_F: GGCAATATATAGGAATGCACGTTTTAGAGCTAGAAATAGCAAGTTAAA
Acg4_12_R: AACACTCGGTATAAATTGGTTTATGCACCAGCCGGGAATCG
Acg4_23_F: GCATAAACCAATTTATACCGAGTGTTTTAGAGCTAGAAATAGCAAGTTAAA
Acg4_23_R: AACTCCCCGCAAGTTCTGTCCCTTGCACCAGCCGGGAATCG
Acg4_34_F: GCAAGGGACAGAACTTGCGGGGAGTTTTAGAGCTAGAAATAGCAAGTTAAA
Acg4_34_R: GGTGGTCTCCGTTTTCCACTTGCACCAGCCGGGAATCG
Acg4_41_F: GTGCAAGTGGAAAACGGAGACCACCGTTTTAGAGCTAGAAATAGCAAGTTAAA
Acg4_41_R: AAAACGTGCATTCCTATATATTGCCTGCATCGGCCGGGAATCG
acgRNA_1_F: ACGTCGGCAATATATAGGAATGCACGTTTTAGAGCTAGAAATAGCAAGTTAAAATAAGG
acgRNA_2_R: AAAACGTGCATTCCTATATATTGCCGACGTTAAATTGAAAATAGGTCTATATATACG
acN_F: CAAACTCATCAATGTATCTTAACCGGTAGGAGCAAGCTGCCCGTGCCCTGGCCCACCCTC
acN_R: GAGGGTGGGCCAGGGCACGGGCAGCTTGCTCCTACCGGTTAAGATACATTGATGAGTTTG
AutoC_Left_F: ACATTATCGCGAGCCGACAGAAGAACGACCCGACAG
AutoC_Left_R: ATTAGATCCCGTACGACGTACCCATTGTTTGCTTTTAATCT
AutoC_Right_F: TATCTTAACCGGCGGAGGTGGCCATATCGCACTACA
AutoC_Right_R: GCAGAAGGCCCCTGACGACGGGCAAGGGAATTCAACA
b1v2_F: ATTTCGAGGTTAAAACGGTCGAAGCGCGGCCGCGGATCTAATTCAATTAGAGACTAATTC
b1v2_R: GAGTAGGAGCAATCACAGGTGAGCAAAAAAACGCGTGTTAACTCGAATCGCTATCCA
Cas9Nos3_R: TATCCACTTGTTTACTCTGACCAACT
Cas9Nos3c_F: TCTGCACCACCGGCTAGCTCCTTCCTGGCCCTTTTCGAG
CFD_1_F: GTTTTAGAGCTAGAAATAGCAAGTTAAAATAAGG
CFD_1_R: GGCTATGCGTTGTTTGTTCTGC
CFD_2_F: AACAGTAGGCAGAACAAACAACGC
CFD35_2_R: CGACGTTAAATTGAAAATAGGTCTATATATACG
CFD5_2_R: TGCATCGGCCGGGAATCGA
CFDg_1_F: GACCTGTTTTAGAGCTTTTTTGCCTACCTGGAGCCT
CFDg_2_R: CAGGTAGGCAAAAAAGCTCTAAAACAGGTCTTCTGCACCA
EGFP_c_F: AAACAATGGGTACGTCGTACGGGATCTAATTCAATTAGAGACTAA
EGFP_c_R: ATATGGCCACCTCCGCCGGTTAAGATACATTGATGAGTTTGG
EGFP1_gRNA_F: TATATATAGACCTATTTTCAATTTAACGTCGAAGTTCGAGGGCGACACC
EGFP1_gRNA_R: ATTTTAACTTGCTATTTCTAGCTCTAAAACGGGTGTCGCCCTCGAACTT
EGFP1Right_F: ATGCGTATGCATTCTAGACCCTGGTGAACCGCATCGAG
EGFP1t_gRNA_F: GCGGCCCGGGTTCGATTCCCGGCCGATGCAGAAGTTCGAGGGCGACACC
EGFP1tt_gRNA_F: GCGGCCCGGGTTCGATTCCCGGCCGATGCAGGTGGTGCAGATGAACTTCA
EGFP1t_gRNA_R: ATTTTAACTTGCTATTTCTAGCTCTAAAACTGAAGTTCATCTGCACCACC
EGFP2_gRNA_F: TATATATAGACCTATTTTCAATTTAACGTCGGGCACGGGCAGCTTGCCGG
EGFP2_gRNA_R: ATTTTAACTTGCTATTTCTAGCTCTAAAACCCGGCAAGCTGCCCGTGCCC
EGFP2Right_F: ATGCGTATGCATTCTAGATCAAGGAGGACGGCAACATCC
EGFP4_12_F: GAAGTTCGAGGGCGACACCCGTTTTAGAGCTAGAAATAGCAAGTTAAA
EGFP4_12_R: AACACAAGCAGAAGAACGGCATCTGCACCAGCCGGGAATCG
EGFP4_23_F: GCAGATGCCGTTCTTCTGCTTGTGTTTTAGAGCTAGAAATAGCAAGTTAAA
EGFP4_23_R: AACGCTTGTGCCCCAGGATGTTGTGCACCAGCCGGGAATCG
EGFP4_34_F: GCACAACATCCTGGGGCACAAGCGTTTTAGAGCTAGAAATAGCAAGTTAAA
EGFP4_34_R: TGAAGTCGATGCCCTTCAGCTGCACCAGCCGGGAATCG
EGFP4_41_F: GTGCAGCTGAAGGGCATCGACTTCAGTTTTAGAGCTAGAAATAGCAAGTTAAA
EGFP4_41_R: AAAACGGGTGTCGCCCTCGAACTTCTGCATCGGCCGGGAATCG
EGFP4Right_F: ATGCGTATGCATTCTAGAAGCAGAAGAACGGCATCAAGGTG

EGFPacLeft_F: ATTAACCAATTCTGAACATTATCGCCTAGGGTACCGACAGAAGAACGACCCGACAG
EGFPacLeft_R: GGCCAGGAAGGAGCTAGCCGGTGGTGCAGATGAACTTCA
EGFPacRg2_R: CAATTTTCCGTTGCACTTTTCGATTTCG
EGFPacRight_F: ATGCGTATGCATTCTAGAGCAAGCTGCCCGTGCCCT
EGFPacRight_R: TGATTGACGGAAGAGCCTCGAGCTGCACACACAGTGGACGGGCAAGGGAATTCAACATCC
EGFPc_U6_3_gRNA1_R: CGGGCAGCTTGCTCTAGAATGCATACGCATTAAGCGAACA
G1Left_R: GCGGCGTTTCTCGAAAAGGGCCAGGAAGGAGCTAGCTGTCGCCCTCGAACTTCAC
gRNA_EGFP1_R: GGTTCACCAGGGTCTAGAATGCATACGCATTAAGCGAACA
gRNA_EGFP1v2_R: GCCCTTCAGCTCGATGCGGTTCACCAGGGTCTAGAATGCATACGCATTAAGCGAACA
gRNA_EGFP2_R: CGTCCTCCTTGATCTAGAATGCATACGCATTAAGCGAACA
gRNA_EGFP4_R: CGTTCTTCTGCTTCTAGAATGCATACGCATTAAGCGAACA
gRNA_f_R: GAGGGTGGGCCAGGGCACGGGCAGCTTGCTCTAGAATGCATACGCATTAAGCGAACA
gRNA_P10_F: AGCTGGCTTGGATAGCGATTCGAGTTAACACGCGTTTTTTTGCTCACCTGTGATTGCTC
gRNAtRNA_F: ACATTATCGCGAGCCTTTTTTGCTCACCTGTGATTGCT
gRNAtRNA_R: CAGAAGGCCCCTGACATGCATACGCATTAAGCGAACA
pBB_1_R: GACCAAAATCCCTTAACGTGAGTT
pBB_2_F: GCGCGTAACTCACGTTAAGG
pBB2_c_F: ATTCCCTTGCCCGTCGTCAGGGGCCTTCTGCTTAGT
pBB2_c_R: GGTCGTTCTTCTGTCGGCTCGCGATAATGTTCAGAATTG
pBBtRNA_1_F: TTAATGCGTATGCATGTCAGGGGCCTTCTGCTTAGT
pBBtRNA_2_R: CAGGTGAGCAAAAAAGGCTCGCGATAATGTTCAGAATTG
U6_3_gRNA1_v4_F: GTCCAAACTCATCAATGTATCTTAACCGGTAGGCCTTTTTTTGCTCACCTGTGATTGCTC

Sequencing primers

AutoC_Left_S_F: AGCAGAGAAAAGTGTAGAGCACG
AutoC_Left_S_R: GTGCTGACCCACGATCCATTC
AutoC_Right_S_F: CCCCCTTCTGCACACCATACA
AutoC_Right_S_R: TACACCTCACACTACTCGGGC
AutoDLeft_S2_F: CTTACGCTGAAGCCATTTCAA
AutoDRight_S2_R: ATCTGGTTCTCACTTCCATTTAAAT
EGFP_S_F: AGCGCACCATCTTCTTCAAGG
EGFP_S_R: AGTTGTACTCCAGCTTGTGCC
EGFP_S2_F: CCCTGAAGTTCATCTGCACCA
EGFP_S2_R: CTCCAGCAGGACCATGTGATC
IHD_S_F: GGGTTATTGTCTCATGAGCGG
IHD_S_R: TCTCGAAAATAATAAAGGGAAAATCAG
pCFD5_S_R: ACGTCAACGGAAAACCATTGTCTA

Generation of transgenic lines. Lines were transformed by Rainbow Transgenic Flies via injection of a donor plasmid (ATSacG, BHDgN1cv3, AHDgN1, THDgN1, AHDgN2, AHDgN2s, AHDgN3, AHDgN4, FACacN, FACacN1, FACacN4) into a w^{1118} (for ATSacG, FACacN, FACacN1, FACacN4) or into the ATSacG line (for the rest). Plasmid pHsp70-Cas9 (*35*) (provided by Melissa Harrison & Kate O'Connor-Giles & Jill Wildonger, Addgene plasmid #45945) was included in the injection as a source of Cas9 and plasmid BHDgg1c (for ATSacG, FACacN, FACacN1, and FACacN4), TTTgU1t (for BHDgN1cv3, AHDgN1, THDgN1), TTTgU2s (for AHDgN2s), or TTTgU4 (for AHDgN2, AHDgN3, AHDgN4) was included as a

source of gRNA. Concentrations in the injection mix of donor, Cas9, and gRNA plasmids were approximately 500, 500, and 50 ng/µL, respectively in 10 mM Tris-HCl, 100 µM EDTA, pH 8.5 solution. Progeny of injected flies with dsRed fluorescent protein in the eyes, which usually indicated successful drive insertion, were crossed to one another for several generations to obtain homozygous stocks, with preference for flies with brighter eyes, which usually indicated that the individual was a drive homozygote. The stock was considered homozygous after sequencing confirmation. The split-CRISPR line with Cas9 driven by the *nanos* promoter and the driving component targeting *yellow* are detailed in a previous study (*15*).

Fly rearing and phenotyping. Flies were reared at 25˚C with a 14/10 hr day/night cycle. Fresh Bloomington Standard Medium was provided every two weeks. For phenotyping, flies were anesthetized with CO_2 and examined with a stereo dissecting microscope. Red and green fluorescent eye phenotypes were scored using the NIGHTSEA system (SFA-GR and SFA-RB-GO). The different phenotypes and genotypes of our drive systems are summarized in the Supplemental Datasets, as are the calculations we used for determining drive performance parameters. The alternate analysis model in the Supplemental Datasets was performed with the lme4 (1.1-21, https://cran.r-project.org/web/packages/lme4/index.html) and emmeans (1.4.2, https://cran.r-project.org/web/packages/emmeans/index.html) packages for the R statistical computing environment (3.6.1). This type of analysis used a binomial generalized linear mixed-effects model to fit the data with linear regression, account for batch effects (from different vials) in our phenotyping (batch effects were found to be small, see Supplemental Data Sets).

Experiments involving gene drive flies were carried out with Arthropod Containment Level 2 protocols at the Sarkaria Arthropod Research Laboratory at Cornell University, a quarantine facility constructed to containment standards developed by USDA APHIS. Additional safety protocols for insect handling were approved by the Institutional Biosafety Committee at Cornell University, further minimizing the risk of unintentional release of transgenic flies. All drive flies also utilized our split-Cas9 system or synthetic target sites(*15*), in order to prevent the spread of the drive in the case of an escape.

Genotyping. To obtain sequences of gRNA target sites, flies were frozen and homogenized in 30 µL of 10 mM Tris-HCl pH 8, 1mM EDTA, 25 mM NaCl, and 200 µg/mL recombinant proteinase K (Thermo Scientific). The solution was incubated at 37˚C for 30 min and then 95˚C for 5 min. The mixture was used as the template for PCR to amplify the gRNA target sites. DNA was then was purified by gel extraction and Sanger sequenced. Sequences were analyzed with ApE software available at: http://biologylabs.utah.edu/jorgensen/wayned/ape.

Genetic computational module. Except in the simple model described in the results section, the flow for DNA modification events in our model is as follows: first, after generating an individual, both of the individual's genes are subject to the formation of resistance alleles in a

germline resistance function that retroactively describes changes that occurred in the germline cells of the parents; next, a homology-directed repair function determines whether an allele was converted to a drive allele; then, there is a second application of the germline resistance function, using a different resistance rate parameter; finally, an embryo resistance function determines whether Cas9 inherited from the mother forms any resistance alleles. Each of these functions, along with a Cas9 cutting function which is invoked by the other functions, is described below.

Germline resistance function:
This function runs on each chromosome, both before and after homology-directed repair. This function first determines a cut rate, and then passes that rate as an argument to a function that represents Cas9 possibly cutting and generating resistance alleles. The function only operates under the threshold conditions that the individual inherited a chromosome with at least one wild type locus from a parent that was a carrier for the drive (necessarily on the parent's other chromosome). If these conditions are met, the rate of cutting is then determined. For a default rate of cutting, this function takes as an argument a global resistance rate as a parameter (see default parameters below).

However, one of the features of this model is the simulation of the possibility of simultaneous cleavage. When this feature of the model is enabled, the cut rate is not simply the resistance rate parameter, but rather, the likelihood of cutting at each subphase is reduced to

$$\text{Subphase cut rate} = 1 - (1 - \text{resistance rate})^{\frac{1}{\text{number of cut phases}}}$$

The subphase cut rate calculation is further modified when simulating Cas9 activity saturation. The per phase cut rate is then calculated as

$$Subphase\ cut\ rate = 1 - (1 - resistance\ rate)^{\frac{Cas\ factor}{number\ of\ cut\ phases * number\ of\ gRNAs}}$$

where

$$Cas\ factor = \frac{Cas9\ saturation\ parameter * number\ of\ gRNAs}{Cas9\ saturation\ parameter + number\ of\ gRNAs - 1}$$

This function undergoes a final modification when our model considers differing gRNA activity level at each different locus. In this case, the function generates a series of cut rates, rather than just one. This variation between rates is based on a global gRNA activity variation parameter. Based on this parameter, a range of gRNA activity multipliers at each target site is constructed as a list with a maximum of (1 + gRNA variation parameter) and a minimum of (1 – gRNA variation parameter), with the number of entries in the list equal to the number of gRNAs. The activity multiplier at each site steps down from the maximum to the minimum in linear steps. The nth cut rate is determined as follows

$$Subphase\ cutrate, site\ N = 1 - (1 - resistance\ rate)^{\frac{Nth\ Cas\ factor}{number\ of\ cut\ phases * number\ of\ gRNAs}}$$

where

$$Nth\ Cas\ factor = \frac{Cas9\ saturation\ parameter\ *\ number\ of\ gRNAs}{Cas9\ saturation\ parameter\ +\ number\ of\ gRNAs\ -\ 1} * nth\ gRNA\ activity\ multiplier$$

After this function has determined the cut rate (or series of cut rates), it is passed as an argument to a Cas9 cutting function described below to determine if a resistance allele forms on the chromosome that the offspring is inheriting from the parent in question.

Embryo resistance function:
The function to determine resistance formation rates in the embryo is highly similar to the function that determines resistance rates in the germline. This function only proceeds when the threshold conditions of the mother being a carrier for the drive and the child having at least one wild type locus are met.

When these conditions are met, the calculations for per phase cut rate differ from those in the germline function only in that the rate is affected by the number of copies of the drive present in the mother. The basic model is

$$Subphase\ cut\ rate\ = 1 - (1 - resistance\ rate)^{\frac{mother\ drive\ count}{number\ of\ cut\ phases}}$$

The function also has one special case. For mothers that are drive/wild type, Cas9 activity has been determined to be higher than for mothers who are drive/resistance (see Supplemental Results). Thus, in the drive/wild-type case, the mother drive count variable is set to 1.83 for individuals that inherited a drive allele from the mother.

When modeling both saturation as well as variable gRNA activity level, the mother drive count has the same place in the resultant cut rate equation. The model including all of these factors calculates the cut rates as

$$Subphase\ cut\ rate\ at\ site\ N = 1 - (1 - resistance\ rate)^{\frac{mother\ drive\ count\ * Nth\ Cas\ factor}{number\ of\ cut\ phases * number\ of\ gRNAs}}$$

where

$$Nth\ Cas\ factor\ =$$

$$\frac{Cas9\ saturation\ parameter\ *\ number\ of\ gRNAs}{Cas9\ saturation\ parameter\ +\ number\ of\ gRNAs\ -\ 1} * nth\ gRNA\ activity\ multiplier$$

After the cut rate has been determined, it is passed as an argument to the Cas cut function which is run on both of the offspring's chromosomes.

End join repair function:
This function takes the cut rates determined by the above functions and modifies the chromosome accordingly. During each of the cut phases, a random number between zero and one is checked against the cut rate for each wild type locus in the offspring's chromosome. If, during any given cut phase, more than one site is cut, the left most locus is marked as a resistance allele that disrupts the function of the target gene, and the rest of the section between the two cuts and including the rightmost cut is marked with a placeholder that represents the absence of this section of DNA. If only one cut is made during a cut phase, the site is converted to either a resistance sequence that disrupts or preserves the function of the target gene at a rate defined by the default model parameters.

Homology directed repair function:
This function determines whether a homing drive successfully copies itself onto the offspring's chromosome. The function runs twice – once considering the offspring's paternal chromosome and the father's genome and once for the maternal chromosome and the mother's genome. The function only runs when the threshold conditions are met of the offspring having a wild type locus on the chromosome it inherited from a parent who was a carrier for the drive. Before considering any of the model's toggleable advanced features, this function flows as follows: First, a cut rate is passed to the function from a homing phase cut rate default parameter. Each wild type locus on the chromosome is checked against that cut rate. If any cuts are made, an additional check is made against a baseline homing success rate parameter. If homing succeeds, the chromosome is converted to a drive chromosome. If a cut is made, but the baseline homing success check fails, end-joining repair occurs. In this case, if multiple loci were cut, the span of DNA is marked as missing, and the first locus is marked as a function disrupting resistance allele. If only one cut is made, either type of resistance sequence can form at the site at rates according to the model parameters.

When modeling gRNA saturation, the cut rate is altered to include the Cas9 saturation factor as well as the number of gRNAs, much like the cut rate is altered in resistance formation. When simulating gRNA saturation, the homology-directed repair cut rate is

$$Cut\ rate\ =\ 1 - (1 - homing\ phase\ cut\ rate\ parameter)^{\frac{Cas\ factor}{number\ of\ gRNAs}}$$

where

$$Cas\ factor\ = \frac{Cas9\ saturation\ parameter\ *\ number\ of\ gRNAs}{Cas9\ saturation\ parameter\ +\ number\ of\ gRNAs\ -\ 1}$$

Just as resistance allele formation can be toggled to vary at each different locus, the cut rates in the homology-directed repair phase can also be modified to reflect variable gRNA activity level at each locus. When toggled on, the cut rates are as follows

$$Cut\ rate\ at\ site\ N\ =\ 1\ -\ (1\ -\ homing\ phase\ cut\ rate\ parameter)^{\frac{Nth\ Cas\ factor}{number\ of\ gRNAs}}$$

where

$$Nth\ Cas\ factor\ = \frac{Cas9\ saturation\ parameter\ *\ number\ of\ gRNAs}{Cas9\ saturation\ parameter\ +\ number\ of\ gRNAs\ -\ 1} \times nth\ gRNA\ activity\ multiplier$$

When Cas9 cut fails to cut out the full span of DNA between the outermost gRNA target sites, imperfect homology due to the excess DNA between the outer target sites and the closest sites that were actually cut results in lower probability of homing occurring successfully (referred to as a repair fidelity penalty). The next toggleable feature of the model is the simulation of these cut offset effects. After it is determined at which loci Cas9 cuts, the model determines how close the left and right cut edges are to the leftmost and rightmost target loci (by considering the index of the cut and also accounting for the fact that segments of the genome may have previously been excised due to simultaneous cutting during resistance formation). The offsets from the actual leftmost and rightmost sites modify the rate of homing success as follows

$$Homing\ success\ rate\ =\ baseline\ success\ parameter\ * (1\ -\ homing\ edge\ effect\ parameter\ *\ left\ offset) (1\ -\ homing\ edge\ effect\ parameter\ *\ right\ offset)$$

For example, consider a genome with 10 target loci. Cas9 has made cuts at sites 3, 4, 6, and 7, and DNA spanning sites 8, 9, and 10 was previously removed and replaced with a single resistance segment (due to prior simultaneous cutting at sites 8 and 10 during resistance formation). Thus, the left side offset is 2 (site three is two away from the actual leftmost locus) and the right offset is 1 (site 7 is the rightmost cut target site, and there is only one locus with any genetic material present to the right of it).

The final toggleable modification in this function is ability to simulate incomplete homology-directed repair. When this feature is enabled, in cases that DNA has been cut, but when the drive has failed to successfully home (i.e. homology-directed repair does not occur), there is a chance that the drive will experience failure in the form of incomplete homology-directed repair. This

converts the allele into a full resistance allele that disrupts the function of the target gene. The odds of this occurring are related to the amount of excess DNA between the cut cuts and the outermost gRNA target sites, as described above. The incomplete homology-directed repair rate is given by

$$Incomplete\ homology\ directed\ repair\ rate = base\ incomplete\ HDR\ rate\ *\ (1 - 0.1\ \times\ left\ offset)(1 - 0.1\ \times\ right\ offset)$$

If incomplete homology-directed repair occurs, then drives with haplolethal or recessive lethal target sites (those with recoded versions of the target gene in the drive) have an additional chance of the allele being converted to a full resistance allele that preserves the function of the target gene due to the recoded region being copied without the drive mechanism and payload being copied as well. The rate of this occurring is

$$Rate\ =\ base\ partial\ HDR\ full\ resistacne\ rate\ *\ (1 +\ right\ offset - left\ offset)$$

The asymmetry in this function between the right and left offsets is because the recoded region is assumed to be on the left end of the homing drive.

Summary of default model parameters

drive homozygote fitness value: 0.9
drive heterozygote fitness value: 0.949
additional gene disruption drive fitness multiplier for individuals with two copies of the drive and/or resistance alleles that disrupt the function of the target gene: 0.95
early germline resistance formation phase cleavage rate: 0.02
late germline resistance formation phase cleavage rate: 0.9
homology-directed repair phase cleavage rate: 0.98
baseline rate at which homology-directed repair (as opposed to end-joining repair) occurs in the homology-directed repair phase after cleavage: 0.95
embryo resistance formation phase cleavage rate: 0.05
chance to form a function preserving resistance allele at a cleavage site: 0.1
number of subphases in resistance formation phases: 3
gRNA activity variation level: 0.2
repair fidelity penalty per step length lacking homology to the drive: 0.055
Cas9 activity saturation level: 1.5
incomplete homology-directed repair baseline rate: 0.1
formation of a complete resistance allele that preserves the function of the target gene if a recoded region is present (haplolethal and recessive lethal drives) and incomplete homology-directed repair takes place rate: 0.001

carrying capacity of the environment: 100,000
drive/wild-type heterozygote release size: 100

Model and data availability. All SLiM configuration files for the implementation of the different models and all simulation data are available on GitHub (https://github.com/MesserLab/Homing_Mechanisms_with_multiplexed_gRNAs).

Supplementary Results

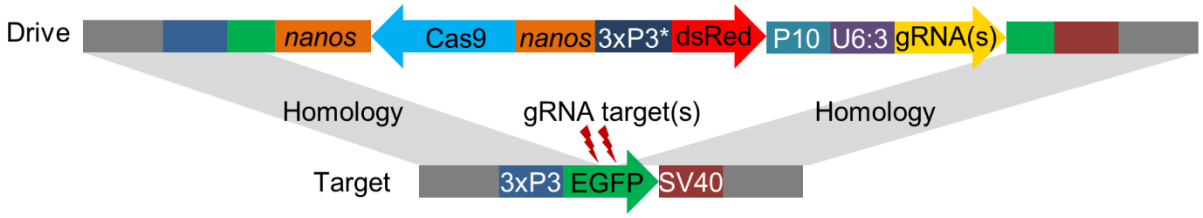

Fig. S1. Synthetic target site drive schematic diagram. The synthetic target site drive constructs contain Cas9 with the germline *nanos* promoter and 3'UTR, a dsRed marker with a slightly recoded (*) 3xP3 promoter and P10 3'UTR, and U6:3 promoter driving one or more tRNA-linked gRNAs that target EGFP. The homology arms include the EGFP target sequence around the outer cut sites together with the 3xP3 promoter and SV40 3'UTR regions.

Cut site sequence analysis

Progeny of drive/wild-type heterozygote females that contained the drive but did not have EGFP phenotype were sequenced to determine the pattern of resistance alleles at each gRNA target site.

Table S1. gRNA cut site sequence analysis.

gRNAs present in mother	Cut site 1	Cut site 2	Cut site 3	Cut site 4	# of sequences with pattern
1,2,3,4	R	mosaic	WT	WT	2
1,2,3,4	R	WT	mosaic	WT	3
1,2,3,4	R	WT	R	WT	3
1,2,3,4	R	WT	WT	mosaic	1
1,2,3,4	R	WT	WT	WT	5
1,2,3,4	R-	-	-	-R	1
1,2,3,4	R-	-	-R	WT	9
1,2,3,4	WT	R	WT	WT	1
1,2,3,4	WT	WT	mosaic	WT	1
1,3,4	R	WT	mosaic	WT	1
1,3,4	R	WT	R	mosaic	1
1,3,4	R	WT	R	WT	1
1,3,4	R	WT	WT	WT	3
1,3,4	R-	-	-R	WT	8
1,3,4	R-	-R	mosaic	WT	1
1,4	R	WT	WT	mosaic	1
1,4	R	WT	WT	WT	6
1,4	R-	-	-	-R	1

WT = wild-type sequence

R = resistance sequence

"-" = large deletion between cut sites

Additional timing components of the model. In our model, resistance alleles are first formed in the early germline. Each wild-type gRNA target site has a 2% probability of being cut. All cuts at this stage undergo end-joining repair, resulting in the formation of resistance alleles. Next is the homology-directed repair phase. Each remaining wild-type site has a 98% probability of being cut. If any sites are cut, homology-directed repair occurs in 95% of cases, resulting in conversion of the entire allele to a drive allele. Otherwise, end-joining repair and formation of resistance alleles takes place as described above. These parameters produce a drive with a conversion efficiency of 91% and inheritance of 96% for one gRNA, which is similar to existing *Anopheles* homing drives (*18*, *19*, *21*, *30*). Finally, since it appears that most wild-type alleles are converted to resistance alleles in the germline (*12*, *13*, *15*), we add another late germline resistance allele formation phase with a high cut rate of 90%, resulting in few wild-type alleles remaining. If, at any stage, multiple sites are cut, the region between them is deleted (preventing future cleavage of deleted gRNA target sites). Overall, in this model, adding additional gRNAs is beneficial, but a maximum efficiency that is determined by the success rate of homology-directed repair is eventually reached (Figure 4).

In addition to those formed in the germline, resistance alleles also form in the early embryo due to maternal deposition of Cas9 and gRNA. Thus, any wild-type alleles obtained from either parent can be cut if the female parent has at least one drive allele, regardless of whether a drive allele was actually inherited by the embryo. If the female has two drive alleles, the enzymatic activity of Cas9 is doubled, which somewhat increases the cleavage rate (see Methods). If the female has a drive allele and the other allele has at least one wild-type site, then it is likely that drive conversion occurs, resulting in increased deposition of Cas9 and gRNA into most embryos receiving the drive allele and thus, increased cleavage. To determine the rate of enzymatic activity in these embryos, we analyzed embryo resistance allele formation rates in the progeny of female drive/wild-type heterozygotes for drives targeting *yellow* (*12*), *white* (*13*), *cinnabar* (*13*), and EGFP (*15*) (also including the lines in this study) in the w^{1118} background, plus additional drives targeting *yellow* that were introduced into the Canton-S (*12*), Global Diversity Line (*12*), and *Drosophila* Genetic Reference Panel (*14*) backgrounds. We found that an enzymatic activity level of 1.83 minimized the sum of squares for the difference between the predicted resistance allele formation in individuals inheriting a drive from a female heterozygote and the actual values. Such predictions were based on the embryo resistance rates in individuals not inheriting a drive allele, which were considered to have a Cas9/gRNA enzymatic activity level of 1. We therefore use this value in our model. We also use a low embryo cut rate of 5%, which appears to be similar to the rate in *Anopheles gambiae* drives using the *zpg* promoter (*21*, *30*).

Additionally, these processes do not necessarily resolve themselves instantaneously. While the window for homology-directed repair is likely narrow, resistance allele formation can occur over an extended period of time either before or after this window. We therefore break up each resistance allele formation phase in both the germline and the embryo into several subphases,

with cut rates adjusted such that the final probability of cutting a particular target site after all subphases are completed is equal to the originally specified cut rate parameter. Greater numbers of subphases result in fewer simultaneous deletions. This can be important for resistance allele formation, but it has a negligible effect on drive conversion efficiency. The effects of this mainly come into play in later generations by controlling the rate that segments are deleted during the formation of resistance alleles. A two-gRNA drive cuts its target sites simultaneously in one third of cases that formed resistance alleles (*13*). We therefore move forward with three subphases for all resistance allele formation phases in our model.

Model with repair fidelity. To model repair fidelity, we modify the probability of successful drive conversion in the homology-directed repair phase. We assume that the reduction in the success rate is proportional to the length of the DNA segment lacking homology and to a repair fidelity penalty parameter. We further assume that gRNA cut sites are evenly spaced, so we measure length in terms of number of cut site intervals, or "steps" between the outer sites and the closest cleavage site. Penalties from left and right homology mismatches are assumed to be multiplicative (see Methods for details). As the penalty increases, additional gRNAs do not contribute substantially to drive conversion efficiency, and overall drive conversion efficiency is reduced (Figure S2). However, though efficiency does not increase, neither is it reduced by a high number of gRNAs (Figure 4), since the cut rate at the outermost gRNAs remains constant.

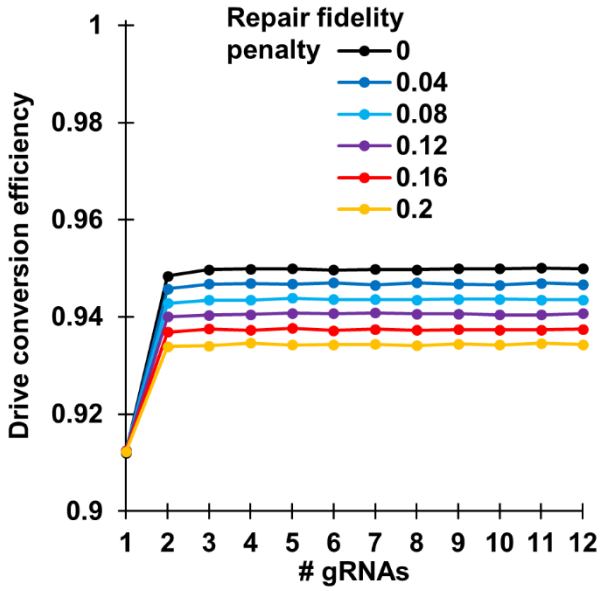

Fig. S2. Effects of repair fidelity on drive performance. Five million offspring were generated from crosses between drive/wild-type heterozygotes and wild-type individuals for each number of gRNAs and each repair fidelity penalty rate. The model includes timing and repair fidelity components, but not other model features. The rate at which wild-type alleles are converted to drive alleles in the germline of drive/wild-type individuals is shown.

We estimated the value of the repair fidelity penalty parameter based on our experimental crosses. Selecting the female *Drosophila* drive/wild-type heterozygotes that have more similar performance to the highly efficient mosquito drives, we note that drive conversion in the drive with a poor right homology arm was 84% the value of the one-gRNA drive with ideal homology arms (Data S3). The right homology arm mismatch was equivalent to our four-gRNA drive if only the first gRNA cut, thus creating a right arm mismatch of three gRNA "steps" in the drive with a poor right homology arm. We therefore estimate the level of mismatch repair fidelity parameter to be a 5.5% efficiency reduction per gRNA step.

Model with and Cas9 activity saturation. To model Cas9 activity saturation, we simply reduce the cut rate per gRNA, with the overall cut rate (total Cas9 enzymatic activity) of all drives increasing asymptotically towards a maximum Cas9 activity level, as specified in the methods section. Since overall cleavage rates plateau, additional gRNAs beyond the first several do not substantially increase the rate of drive conversion (Figure 4, Figure S3).

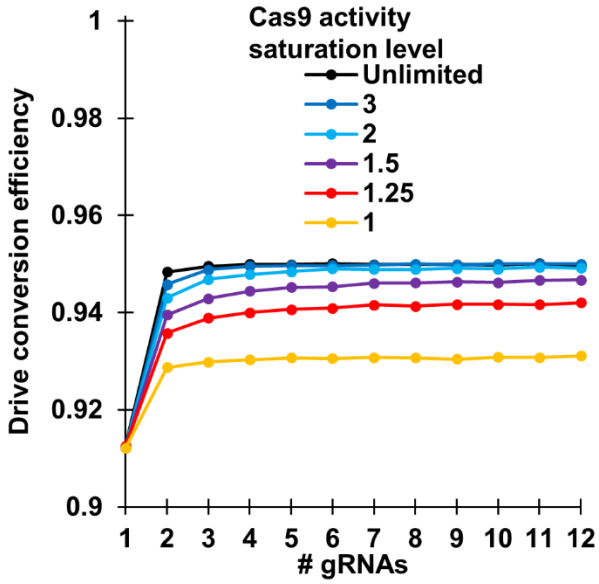

Fig. S3. Effects of Cas9 activity saturation on drive performance. Five million offspring were generated from crosses between drive/wild-type heterozygotes and wild-type individuals for each number of gRNAs and each Cas9 activity saturation level. The model includes timing and Cas9 activity saturation components, but not other model features. The rate at which wild-type alleles are converted to drive alleles in the germline of drive/wild-type individuals is shown.

To estimate the Cas9 activity saturation parameter, we have two methods, each based on examining embryo resistance. First, using the split-*yellow* drives (Data S4) and taking into account the copying of the gRNA (making its quantity equal to 1.83 times the quantity of other individual gRNAs for embryo resistance in individuals inheriting the drive, see timing section), we obtain values of 1.5 and 3.7 comparing the one-gRNA split-Cas9 and four-gRNA split-Cas9 alleles respectively to the baseline provided by the split-Cas9 without any gRNAs. However, the *yellow* gRNA is expressed at a different genomic location and without the tRNA system of the other gRNAs, which potentially accounts for the wide discrepancy between the two values. Another way to assess this parameter is to compare the embryo resistance of the one-gRNA drives with a tRNA to the embryo resistance rate of two-gRNA drives. This is because the second gRNA in each of these drives provides negligible cutting compared to the first in the embryo (Table S1). In our analysis, we focus on embryo resistance in flies that do not inherit the drive allele because Cas9 activity is overall lower, allowing a reduction in cleavage rate to be detected more easily despite the lower number of counts for these groups. This yields Cas9

maximum activity parameters of 1.6, 1.2, 1.9, and 1.5 when comparing the standard one-gRNA drive to the further spaced two-gRNA drive, the standard one-gRNA drive to the closely spaced two-gRNA drive, the one-gRNA drive with poor right end homology to the further spaced two-gRNA drive, and the one-gRNA drive with poor right end homology to the closely spaced two-gRNA drive, respectively. We therefore proceed with an estimate of 1.5 for the maximum Cas9 activity saturation level parameter.

Model with varying gRNA activity level. As indicated in our experiments, the relative activity levels of gRNAs can vary considerably, even if all are expressed together at presumably the same levels. We thus added a simplified version of gRNA activity variance to our model. This is based around a parameter that modifies the enzymatic activity level of each gRNA (see Methods). The left gRNA has its activity increased by a gRNA activity variance parameter, and the right gRNA has its activity decreased by this amount. Middle gRNAs are linearly stepped down in activity from left to right. With increasing gRNA activity variance, cleavage at gRNA sites near the right end is reduced, resulting in lower drive conversion due to the imperfect fidelity repair penalty (Figure S4). gRNAs with particularly low activity are unlikely to be used in drives designed for deployment in natural populations, but it is likely that there would still be some variance in gRNA activity. We thus selected 0.2 as the default parameter for gRNA activity variance, which has a small negative effect on drive conversion efficiency (Figure 4).

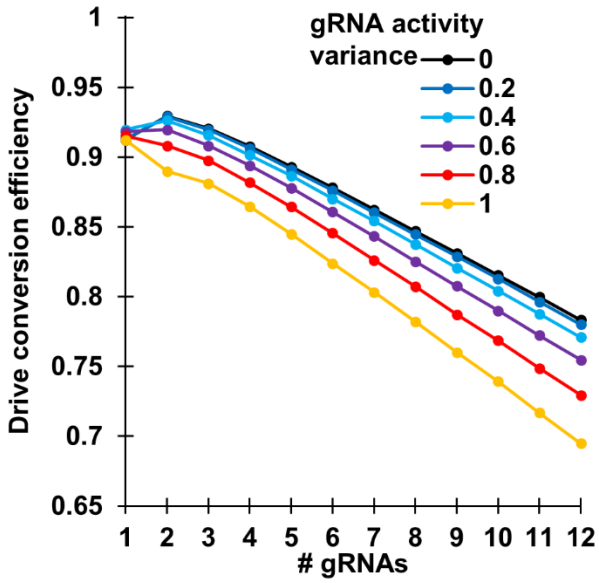

Fig. S4. Effects of gRNA activity variance on drive performance. Five million offspring were generated from crosses between drive/wild-type heterozygotes and wild-type individuals for each number of gRNAs and each gRNA activity variance level using the full model. The rate at which wild-type alleles are converted to drive alleles in the germline of drive/wild-type individuals is shown.

Incomplete homology-directed repair. Previous work has shown that some resistance alleles can be formed when homology-directed repair is interrupted, leaving a short sequence from the drive allele that is sufficient to disrupt any target gene and prevent future Cas9 cleavage. Based on sequencing, approximately 3% of resistance alleles for a drive targeting *yellow* (*12*) and 7% for a drive targeting *white* (*13*) were alleles formed by incomplete homology-directed repair. We thus model that in the homology-directed repair phase, if drive conversion does not occur, there is a 5% chance that incomplete homology-directed repair occurs, which converts all target sites into resistance alleles, even where cleavage did not take place. This chance is slightly increased if there is mismatch between ends in the same manner that drive conversion is decreased due to reduced repair fidelity (see Methods). This is because homology-directed repair may start at one chromosomal end with good homology only to fail at the other end where poor homology makes the process more difficult, resulting in incomplete homology-directed repair before end-joining mechanisms finish repair of the DNA. In most cases, incomplete homology-directed repair does not substantially increase the number of resistance alleles formed. However, due to the specific type of resistance alleles formed, it can have a substantial effect on the family of drives that disrupt an essential target gene while providing rescue by carrying a recoded version of the gene.

In these drives, resistance alleles that disrupt the function of the target gene either do not enter the population or carry high fitness costs. However, in such drives, incomplete homology-directed repair could result in copying of the recoded portion of these drives without copying the drive's replication mechanism. This results in the formation of a complete resistance allele that preserves the function of the target gene. In our model, we include a parameter representing the chance that this occurs, given that incomplete homology-directed repair occurs. It is likely to be a rare phenomenon, but with even low rates, the formation rate of resistance alleles that preserve the function of the target gene substantially increases in drives with several gRNAs (Figure 5). With little information to estimate this parameter, we assume a default value of 0.1%. This places the rate on the order of the chance that a payload gene would be inactivated by mutations that form during homology-directed repair (estimated as approximately one in ten thousand per instance of homology-directed repair of the drive (*36*)).

Effect of cleavage rates on the performance of multiple gRNA homing drives. Our analysis used parameters inspired by highly efficient gene drives in *Anopheles*. However, less efficient drives could still succeed in modifying or suppressing populations. Such drives may have a different optimal number of gRNAs. To investigate this, we examined a drive with similar performance to our synthetic target site drives in *D. melanogaster* which were constructed in this study, albeit assuming an improved promoter with a reduced rate of embryo resistance allele formation. Specifically, the early germline resistance allele formation phase cleavage rate was increased from our default of 2% to 5%. The homology-directed repair phase cleavage rate was reduced from 98% to 92%, and the embryo resistance allele formation phase cleavage rate was increased from 5% to 10%. With these parameters, the performance of population modification drives was moderately worse, as expected (Figure S5). The optimal number of gRNAs for most of the drives was increased from three to four, and the negative effects of a high number of gRNAs were more pronounced. The success rates of suppression drives were more drastically impacted by gRNA count (Figure 7).

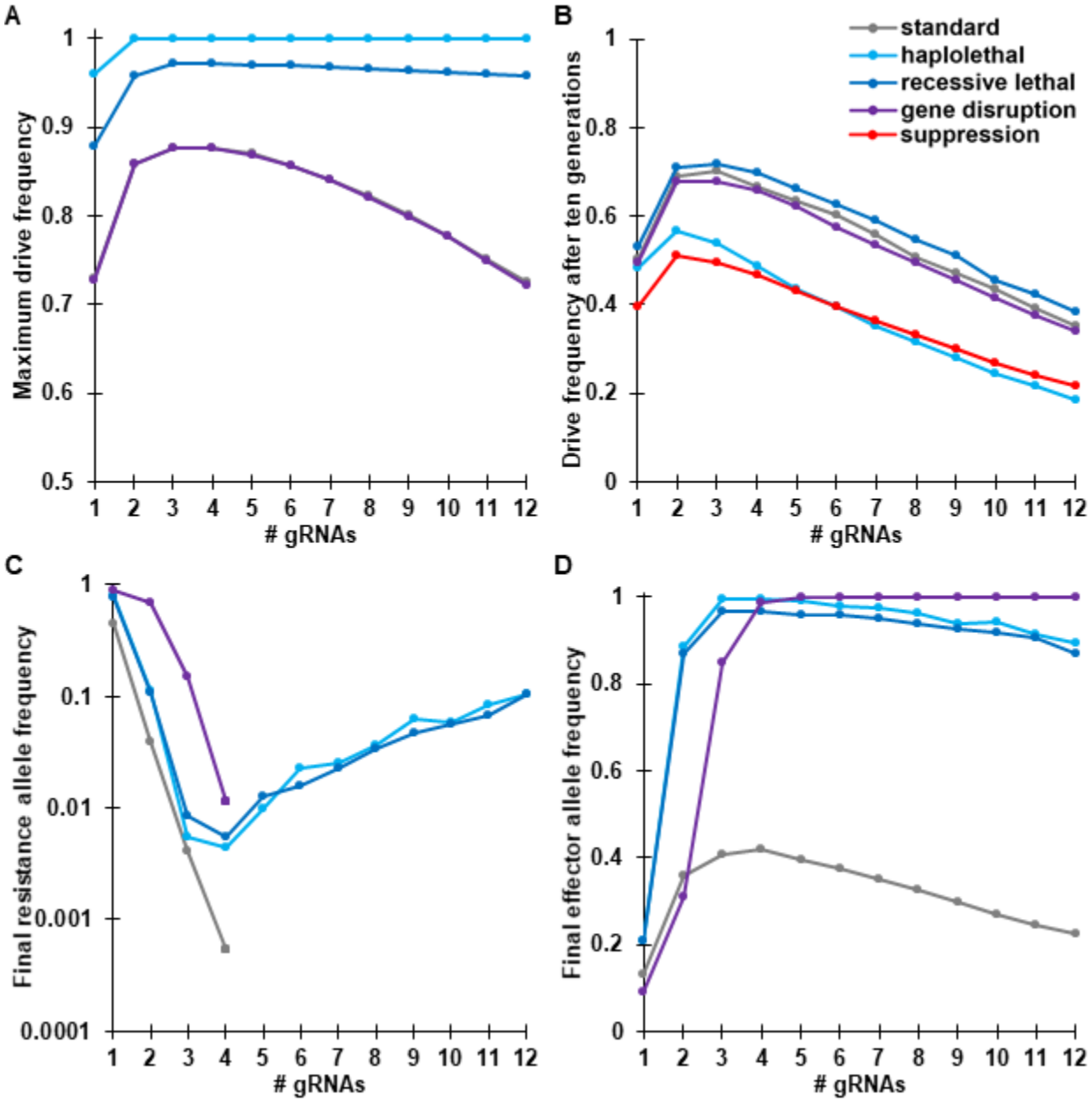

Fig. S5. Comparison of performance parameters for different types of homing drives with lower cleavage efficiencies. Drive/wild-type heterozygotes were released into a population of 100,000 individuals at an initial frequency of 1%. The simulation was then conducted for 100 generations using the full model, but with reduced drive efficiency compared to the default parameters. The displayed results are the average from 20 simulations for each type of drive and number of gRNAs (**A**) The maximum drive allele frequency reached at any time in the simulations. Note that the standard drive and gene disruption drive values are highly similar. (**B**) The number of generations needed for the drive to reach at least 50% total allele frequency. Note that the suppression drive is only shown in (**B**). (**C**) The final frequency of resistance alleles after 100 generations. The displayed values are only for resistance alleles that preserve the function of the target gene. No resistance alleles were present in the standard drive and gene disruption drive when at least four gRNAs were present. (**D**) The final effector frequency present in the population after 100 generations. This was the drive allele only for most drive types, but for the gene disruption drive, it includes resistance alleles that disrupt the function of the target gene as well.

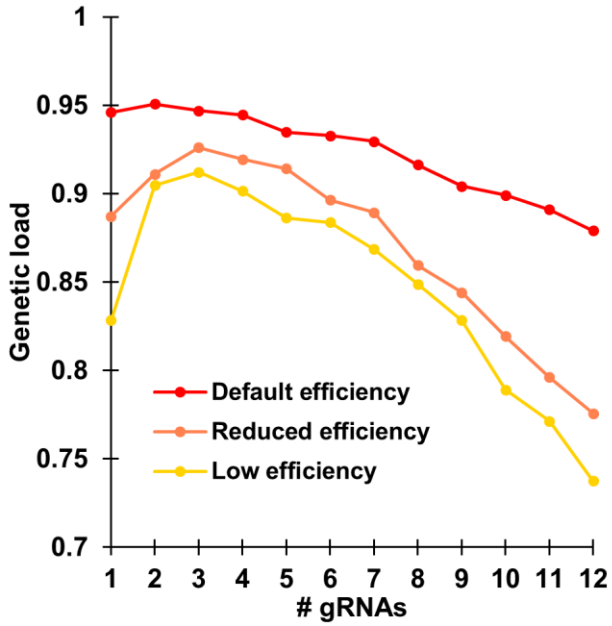

Fig. S6. Genetic load. Drive/wild-type heterozygotes with a suppression drive were released into a population of 100,000 individuals at an initial frequency of 1%. The simulation was then conducted for 100 generations for each type of drive and number of gRNAs. Fertile individuals were allowed to have more offspring to prevent complete suppression and allow measurement of the genetic load. The displayed results are the average genetic over the last 50 generations. The genetic load is defined as 1 - (number of offspring in the current generation / expected number of offspring based on the previous generation assuming that all individuals were wild-type) and is a measure of the suppressive power of the drive. The full model was used, but the rate of resistance sequences preserving the function of the target gene was set to zero. The default system based on *Anopheles* parameters used an early germline cleavage rate of 2%, a homology-directed repair phase cleavage rate of 98%, and an embryo cleavage rate of 5%. For the reduced efficiency drive model, these parameters were changed to 5%, 92%, and 10%, respectively. The low efficiency drive model changed these parameters to 8%, 90%, and 15%, respectively.

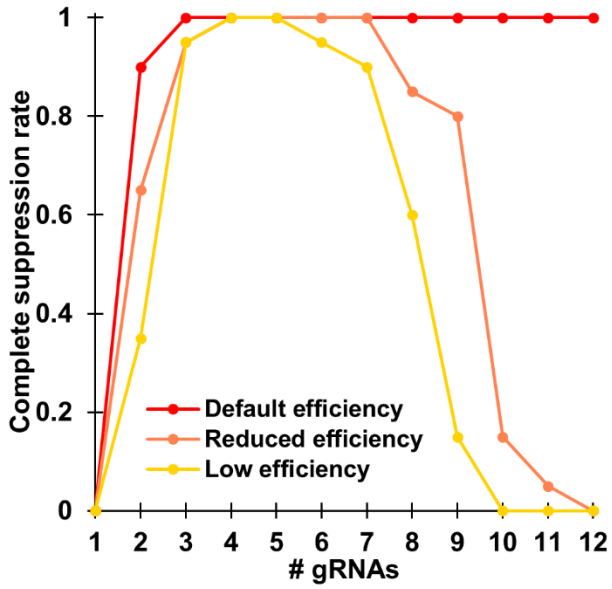

Fig. S7. Number of gRNAs needed for successful population suppression with a reduced functional resistance rate. Drive/wild-type heterozygotes with a suppression drive were released into a population of 100,000 individuals at an initial frequency of 1%. The simulation was then conducted for 100 generations. The displayed results are the average from 20 simulations for each type of drive and number of gRNAs. The fraction of simulations that resulted in successful suppression are shown. The full model was used as in Figure 7A, but the rate of resistance sequences preserving the function of the target gene was reduced from the default value of 0.1 to a lower value of 0.01. The default system based on *Anopheles* parameters used an early germline cleavage rate of 2%, a homology-directed repair phase cleavage rate of 98%, and an embryo cleavage rate of 5%. For the reduced efficiency drive model, these parameters were changed to 5%, 92%, and 10%, respectively. The low efficiency drive model changed these parameters to 8%, 90%, and 15%, respectively.